

Tuning Metal–Organic Framework (MOF) Topology by Regulating Ligand and Secondary Building Unit (SBU) Geometry: Structures Built on 8-Connected M_6 ($M = \text{Zr}, \text{Y}$) Clusters and a Flexible Tetracarboxylate for Propane-Selective Propane/Propylene Separation

Xingyu Li,[†] Jiaqi Liu,[†] Kang Zhou, Saif Ullah, Hao Wang,* Jizhao Zou,* Timo Thonhauser, and Jing Li*



Cite This: *J. Am. Chem. Soc.* 2022, 144, 21702–21709



Read Online

ACCESS |



Metrics & More

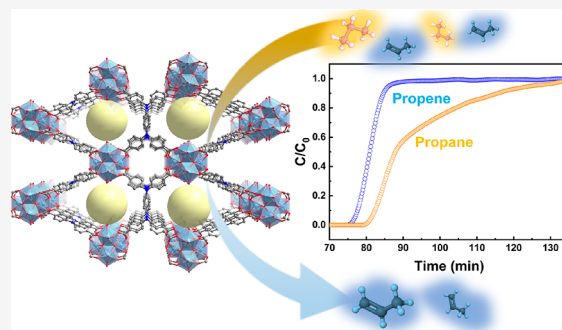


Article Recommendations



Supporting Information

ABSTRACT: Topology evolution originating from variations of linker and SBU (Secondary Building Unit) geometries could largely enrich the chemistry of metal–organic frameworks (MOFs). Here we report the synthesis and characterization of three MOF structures built on the same organic linker, *N,N,N',N'*-Tetrakis(4-carboxyphenyl)-1,4-phenylenediamine (tcppda) and similar 8-connected M_6 ($M = \text{Zr}$ or Y) clusters. The three compounds, HIAM-402, HIAM-403, and HIAM-311, feature 4,8-connected *sqc*, *scu*, and *flu* topology, respectively. Detailed structural analysis revealed that different geometries of the inorganic M_6 SBUs as well as the organic linker have led to the formation of distinct MOF nets. In particular, HIAM-402 features exceptional framework stability and high porosity and acts as a propane-selective adsorbent for the discrimination of propane and propylene. Its balanced adsorption selectivity ($S_{\text{propane/propylene}} = 1.43$) and capacity ($Q_{\text{propane}} = 133.3 \text{ cm}^3/\text{g}$, 298 K and 1 bar) endow it with the capability of separating propane and propylene mixtures and one-step production of highly pure propylene (purity >99.9%), as validated by column breakthrough measurements, with the presence of moisture or propyne. *Ab initio* calculations further confirm that the propane-selective behavior of HIAM-402 is a result of its higher binding energy toward propane compared to that of propylene.



INTRODUCTION

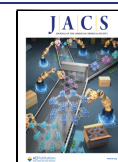
Metal–organic frameworks (MOFs) represent a fascinating type of multifunctional crystalline porous materials which have attracted tremendous attention from both academia and industry over the past two decades.¹ The intriguing features of MOFs lie primarily in their great promise for various applications as well as unprecedented, rich chemistry. The potential applications of MOFs have spread from gas storage/separation,^{2–6} catalysis,^{7,8} to food preservation,^{9,10} and environmental protection.^{11–14} Endeavors are being made for the industrial implementation of MOFs in related fields.¹⁵ On the other hand, the structure diversity, framework flexibility, tunable pore structure, and functionality of MOFs have brought exciting chemistry findings.^{16,17}

Compared to traditional inorganic adsorbents such as zeolites which have limited structure types, the most prominent feature of MOFs is their structural diversity. Assembled from inorganic metal ions/clusters and organic linkers, MOFs can have, in theory, a countless number of structures, by combining metal nodes and organic struts in different ways. In general, three strategies have been used in the customized synthesis of new MOFs: linker engineering,

metal/SBU engineering, and linker conformation engineering.¹⁸ The former two have been repeatedly practiced, in particular with the guidance of reticular chemistry, where MOFs with precisely tailored structure/functionality and/or MOFs featuring novel topology could be achieved.^{19–21} The latter, developing new MOFs by engineering the conformation of organic linkers, has not been documented until recently. In recent studies, Liu, Farha, Zhou and co-workers have demonstrated the realization of different MOF structures built on Zr_6 clusters and tetatopic carboxylate linkers featuring different conformations for inorganic nodes and/or organic linkers.^{18,22,23} This may lead to a new direction where structural diversity of MOFs could further be enriched.

Received: September 5, 2022

Published: November 2, 2022



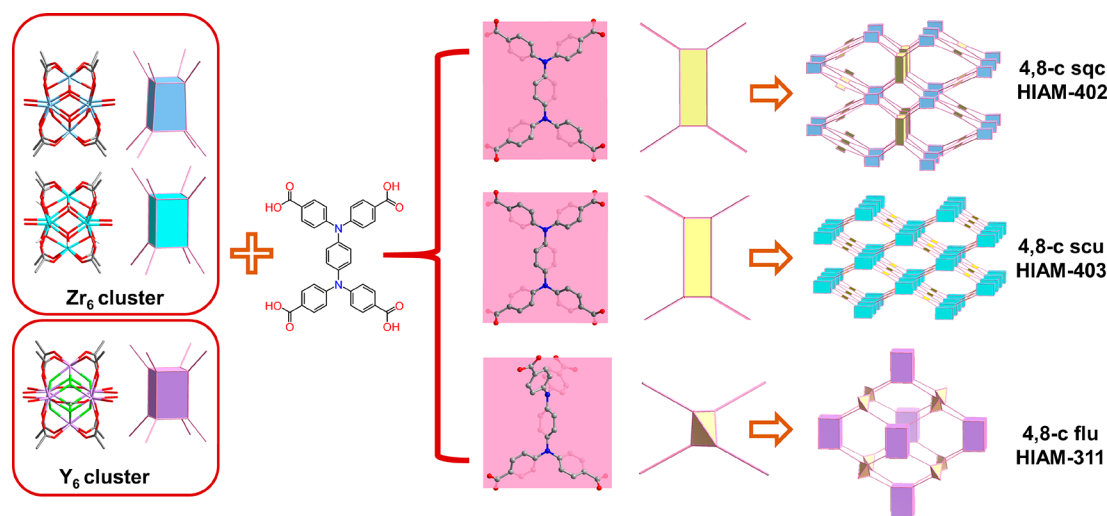


Figure 1. Structure and topology of HIAM-402, HIAM-403, and HIAM-311. Atom color scheme: O, red; C, gray; F, light green; Zr, pale blue or cyan; Y, lavender.

Among various applications that MOFs have been evaluated for, olefin/paraffin separation, in particular the discrimination of propane and propylene, has been the main focus.^{2,24–27} This is due to the paramount importance of propane/propylene separation in the chemical industry, as well as the highly tunable pore structure of MOFs making them particularly suitable for this challenging separation. To date, a number of MOFs have demonstrated the capability of separating propane and propylene via selective adsorption of propylene over propane, either by the introduction of propylene-selective open metal sites (OMSs)²⁸ or through kinetically controlled size exclusion.^{2,25–27} While some of the adsorbents exhibit relatively high adsorption capacity and/or selectivity, the proposed separation strategy suffers from complicated adsorption–desorption cycles as well as a high energy penalty associated with adsorbent regeneration. In this regard, using propane-selective adsorbents for propane/propylene separation could ideally produce highly pure propylene directly in one single step, largely simplifying the process and lowering the energy input. However, in comparison with the explosive growth of reported ethane-selective MOFs (over ethylene),^{24,29–32} propane-selective adsorbents (over propylene) are scarce. This could be attributed to the high similarity between propane and propylene with respect to their physical properties. Only a few propane-selective adsorbents have been validated for one-step production of highly pure propylene from a propane/propylene mixture.^{33–36} Development of novel propane-selective adsorbents with balanced adsorption selectivity and capacity, and the ability for one-step purification of propylene from propane/propylene or even propane/propylene/propyne mixtures, remains a daunting challenge.

Herein, we report a series of three MOFs featuring 4,8-connected **sqc**, **scu**, and **flu** topology, respectively. All three are built on similar 8-connected hexanuclear Zr_6/Y_6 clusters and the same organic linker. Detailed structural analysis revealed the distinct topology of the three compounds originate from their different conformations of the inorganic SBUs and/or the organic linker. The three MOF structures show very different stability and porosity. In particular, HIAM-402 possesses a highly robust framework as well as high porosity and exhibits selective adsorption of propane over propylene. Experimental breakthrough measurements have demonstrated the capability

of HIAM-402 for one-step production of high-purity propylene from propane/propylene and propane/propylene/propyne mixtures. The underlying mechanism of its propane-selective behavior has been explained by *ab initio* computational modeling.

RESULTS AND DISCUSSION

Synthesis and Structure. All three compounds (HIAM-402, HIAM-403, and HIAM-311) were synthesized solvothermally at 120 °C, using the same amount of inorganic salts ($ZrCl_4$ or $Y(NO_3)_3 \cdot 6H_2O$) and organic ligand ($H_4tcppda$), but with different acid modulators and solvents (see [Supporting Information](#) for synthetic details, [Figure S1](#)), and their structures were analyzed by single-crystal X-ray diffraction studies. HIAM-402 was synthesized in DMF with the addition of trifluoroacetic acid, which was obtained as polyhedral-shaped crystals. The compound crystallizes in a tetragonal crystal system with a space group of $I4_1/amd$ ([Table S1](#)). It is built on a 8-connected $Zr_6(\mu_3-O)_4(\mu_3-OH)_4(COO)_4$ SBU, and the remaining four connection sites are occupied by terminal OH^-/H_2O . The inorganic clusters are interconnected through $tcppda^{4-}$ to form the resulting 3D network featuring **sqc** topology ([Figure 1](#)). In the framework of HIAM-402, there are two types of 1D channels, with pore dimensions of $11.4 \text{ \AA} \times 4.0 \text{ \AA}$ and $8.4 \text{ \AA} \times 18.6 \text{ \AA}$, respectively ([Figure S2](#)). The overall formula of the compound is $Zr_6(\mu_3-O)_4(\mu_3-OH)_4-(tcppda)_2(OH)_4(H_2O)_4$.

HIAM-403 was prepared in DMA in the presence of formic acid, and prismatic-shaped crystals were obtained ([Figure S1](#)). Single-crystal X-ray diffraction analysis revealed the compound crystallizes in the orthorhombic crystal system with a space group of $Cmmm$ ([Table S2](#)). HIAM-403 possesses the same connectivity and molecular formula as those of HIAM-402. However, it features a **scu** topology, as a result of the different geometries of the SBU and the linker, which will be discussed later. In the crystal structure of HIAM-403, there exists 1D rhombic channels of $10.1 \text{ \AA} \times 22.9 \text{ \AA}$ along the *c*-axis ([Figure S3](#)).

By combining $Y(NO_3)_3 \cdot 6H_2O$ with $H_4tcppda$ in DMF (or DMA) and water, with the addition of 2-fluorobenzoic acid, we obtained cubic crystals of HIAM-311. It crystallizes in the orthorhombic crystal system with a space group of $Fmmm$

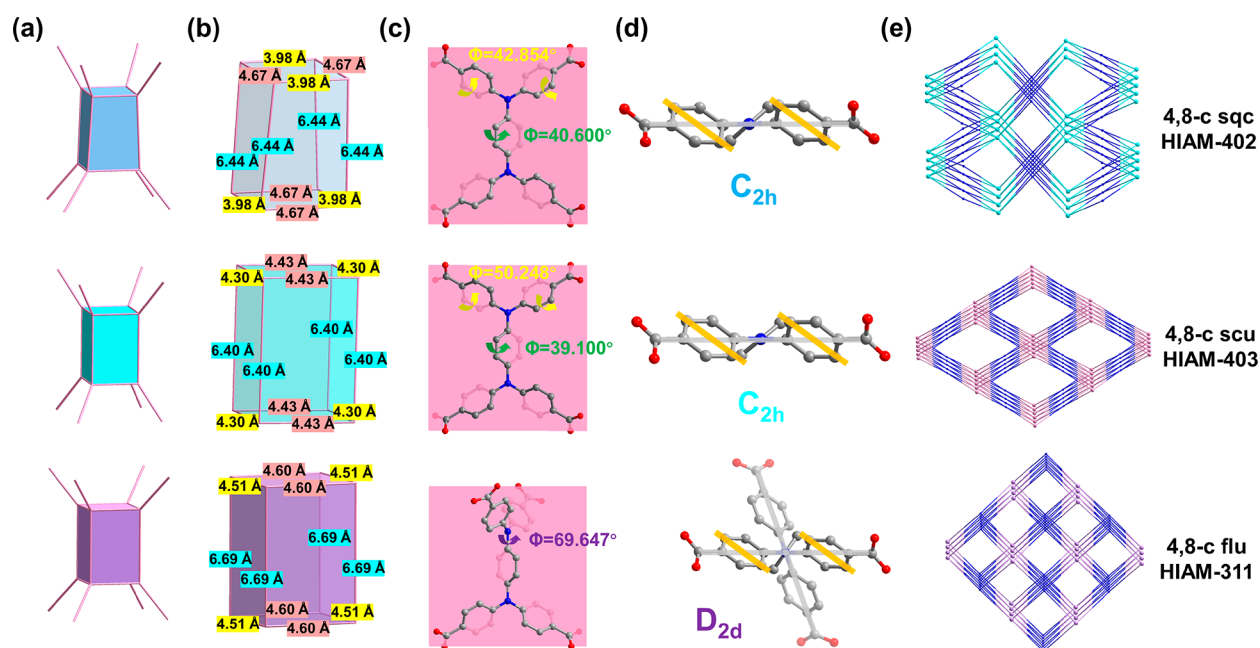


Figure 2. Geometries of the M_6 cluster and the $tcppda^{4-}$ linker in the three MOFs. (a and b) Geometries of the cuboids formed by connecting carbon atoms of the eight adjacent carboxylates that are bonded to the same hexanuclear SBU. (c and d) Geometries of the organic linker. In (d) the gray lines represent the relative orientation of the plane formed by connecting the carboxylate carbon atoms with sp^3 N atom and the yellow lines depict the relative orientation of the deviation of the benzoate from the plane. (e) Nets of the three compounds.

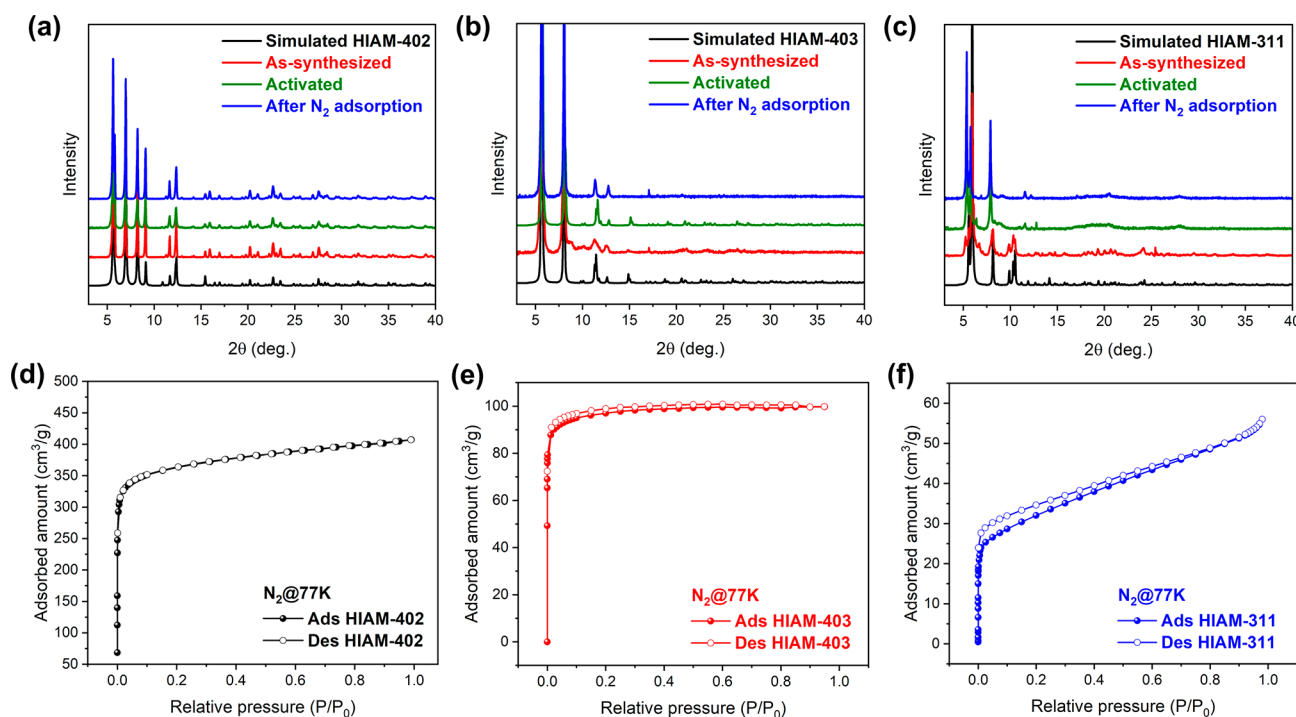


Figure 3. PXRD patterns of (a) HIAM-402, (b) HIAM-403, (c) HIAM-311, and N_2 adsorption–desorption isotherms of (d) HIAM-402, (e) HIAM-403, and (f) HIAM-311 at 77 K.

(Table S3). Similar to HIAM-402 and HIAM-403, HIAM-311 is built on 8-connected hexanuclear Y_6 clusters propagated by $tcppda^{4-}$, with a formula of $Y_6(\mu_3-F)_8(tcppda)_2(HCOO)_4(H_2O)_4$. Unlike that of the aforementioned Zr-based analogs, HIAM-311 features 4,8-c flu topology due to the high deformation of the organic ligand into a tetrahedral geometry. There are intersecting 1D channels along all three crystallographic axes (Figure S4).

Geometries of the SBU and the Linker. While the title compounds (HIAM-402, HIAM-403, and HIAM-311) are exclusively built on 8-connected Zr_6 or Y_6 clusters and the 4-connected $tcppda^{4-}$ linker, they feature distinctly different topologies which largely influence their framework stability and porosity. This encouraged us to analyze the structural differences in detail. Indeed, we found the different topologies originate from the geometry of the SBU as well as the organic

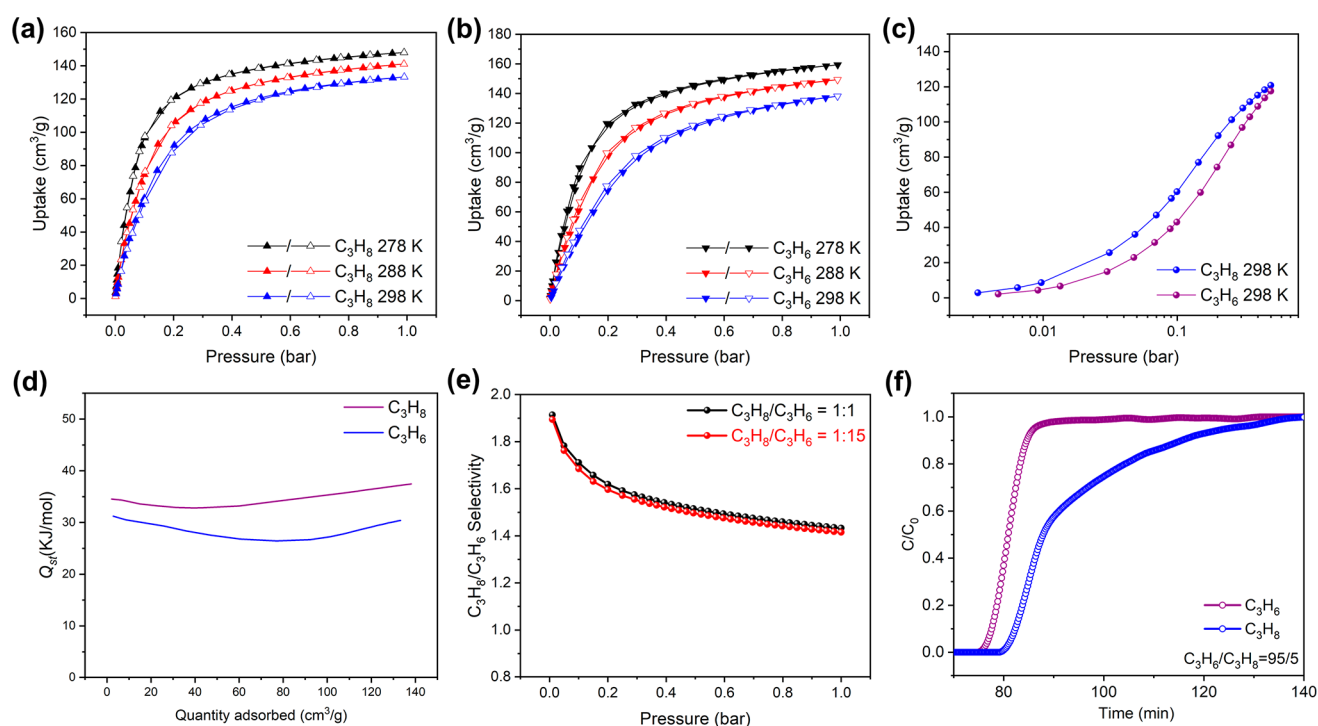


Figure 4. Single-component adsorption–desorption isotherms of (a) propane and (b) propylene at 278, 288, and 298 K on HIAM-402. (c) Comparison of C_3H_8/C_3H_6 adsorption isotherms at 298 K. (d) Isosteric heats of adsorption of C_3H_8 and C_3H_6 . (e) IAST adsorption selectivity of C_3H_8/C_3H_6 (1/1 and 1/15; v/v) on HIAM-402. (f) Dynamic breakthrough curves of HIAM-402 for C_3H_8/C_3H_6 (5/95; v/v) at 298 K and 1 bar.

linker in each structure, which dictates the type of resultant nets.

We first looked into the hexanuclear M_6 octahedra of the inorganic SBU (Figure S5). In general, the two Zr_6 octahedra in HIAM-402 and HIAM-403 are similar except for the slight difference in the distances of the adjacent Zr ions. In comparison, the Y_6 octahedron in HIAM-311 is somewhat larger than the Zr_6 octahedra in the other two Zr-based structures. The diagonal Y–Y distance is 5.53 Å, longer than that for Zr–Zr which is 5.01 Å. This could be attributed to the larger cation radius of Y(III) than that of Zr(IV). No notable distortion was observed for any of the hexanuclear cores. We then examined the coordination environment of the M_6 by comparing the cuboids formed by connecting carbon atoms of the eight adjacent carboxylates that are bonded to the same hexanuclear SBU (Figure 2a and 2b). In particular, the cuboid of HIAM-402 is noticeably distorted, compared to those of HIAM-403 and HIAM-311. Also, it is observed that the dimensions of the cuboid in HIAM-311 are larger than those of the other two structures.

Compared to the geometry of the inorganic SBUs, the organic linker $tcppda^{4-}$ is of high flexibility due to the two sp^3 N atoms. It adopts notably different configurations in the three MOF structures. In both HIAM-402 and HIAM-403, the linker has a C_{2h} symmetry (Figure 2c and 2d). But the benzoate arms are twisted at different degrees (highlighted in yellow in Figure 2c, depicted by the angle between the benzoate plane and the plane formed by connecting the four carboxylate carbon atoms). The distortion is more severe in HIAM-403 with a twisting angle of 50.248°, higher than that for HIAM-402 (42.854°). In addition, the central phenyl ring also deviates from the plane connecting the four carboxylate carbon atoms by 40.6° and 39.1° for HIAM-402 and HIAM-403, respectively (highlighted in green in Figure 2c). Despite the deformation,

the four carboxylates of the $tcppda^{4-}$ linker are coplanar in both structures. In contrast, the ligand in HIAM-311 is highly distorted, resulting in a tetrahedral geometry of the four carboxylates and a D_{2d} symmetry of the linker. Such a geometry leads to the formation of *flu* topology (Figure 2e). It should be noted that the different geometries of the SBUs and the linkers in these structures leading to their unique framework topologies are the results of the different synthetic conditions, such as solvent types, amounts of acid modulators, etc. The correlations between synthetic conditions and the self-assembly of products with different nets were studied in a recent work.¹⁸

Stability and Porosity. Phase purities of the title compounds were confirmed by powder X-ray diffraction (PXRD) analysis. The experimental patterns match well with the simulated ones (Figure 3a–3c). Thermogravimetric analysis (TGA) displayed that all three structures have notable weight losses at relatively low temperature, corresponding to free solvents inside the channels (Figure S6). Weight losses associated with structural decomposition were observed at 400–500 °C (Figure S7). While the three compounds are built on similar hexanuclear clusters and the same organic ligand, we envisioned they may have different stability due to the different degrees of distortion of the inorganic and organic building blocks, as well as the different packing (topology).

To evaluate the chemical and thermal stability of the three compounds, the as-synthesized materials were treated under various conditions. In general, all three compounds maintained their overall structural integrity upon solvent removal and subsequent gas adsorption (Figure 3a–3c). However, loss of high-angle peaks was observed for HIAM-403 and HIAM-311, indicating their relatively low stability. Stability tests were further performed on samples immersed in water and subjected to long-term heating or organic solvent treatments

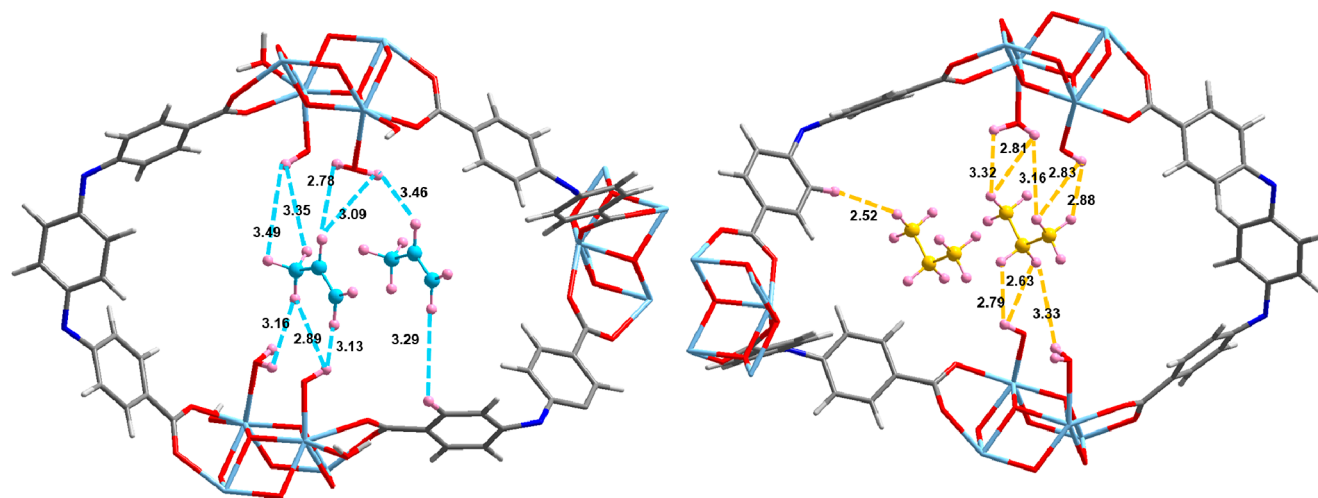


Figure 5. Optimized configuration of adsorbed C_3H_6 (left) and C_3H_8 (right) in the channel of HIAM-402 by *ab initio* calculations.

(Figure S8). The results show that HIAM-402 possesses strikingly high framework robustness. Its crystal structure was fully retained after 1 year on the shelf, 1 week at 150 °C in the open air, or 3 weeks in water. In contrast, the other two compounds underwent partial structural degradation upon similar treatments. Considering the similar SBU and the same organic linker applied in the three compounds, their difference in framework stability could be attributed to the conformation and packing of organic linkers.

The porosity of the three compounds was evaluated by nitrogen adsorption at 77 K (Figure 3d–3f, Figure S9). They all display Type I adsorption profiles, suggesting their microporous nature. In particular, HIAM-402 shows a saturation capacity of 407 cm^3/g , giving a BET surface area of 1442 m^2/g and a pore volume of 0.61 cm^3/g . The pore size distribution curve displays two peaks at 8 and 12 Å, close to the pore size measured from the crystal structure (Figure S10). Three successive cycles of the adsorption–desorption of N_2 at 77 K were performed on HIAM-402 and no notable loss of adsorption capacities and porosity was observed, indicating its framework robustness (Figure S11). In contrast, HIAM-403 and HIAM-311 exhibit substantially lower porosity, with BET surface areas of 384 and 113 m^2/g , respectively. These numbers are notably lower than the theoretically predicted values which could be attributed to their relatively low framework stability that may cause partial structural degradation upon solvent removal.

Adsorption and Separation of Light Hydrocarbons.

Adsorption and separation of light hydrocarbons were evaluated for HIAM-402 in view of its high porosity as well as robust framework. Column breakthrough measurements show that HIAM-402 can extract methane from a six-component (CH_4 , C_2H_2 , C_2H_4 , C_2H_6 , C_3H_6 , and C_3H_8) mixture, which may find use in natural gas purification (Figure S12). It was also noticed that HIAM-402 preferentially adsorbs propane over propylene. This prompted us to look further into its adsorption and separation performance over the two gases, as propane-selective adsorbents have been rarely reported but are more desirable for energy-saving industrial separation processes. Single-component adsorption–desorption isotherms of propane and propylene at 278, 288, and 298 K were collected (Figure 4a–4b). The adsorption capacities for the two gases are ~ 130 – $140 \text{ cm}^3/\text{g}$ at 298 K and 1 bar, higher

than those of most MOF materials and comparable to those of the benchmark adsorbent MOF-74 series.²⁸ At a relatively low pressure region, propane is notably more favored by HIAM-402 (Figure 4c). This could naturally be attributed to thermodynamically driven discrimination due to different adsorption affinity. Isothermic heats of adsorption (Q_{st}) calculated from adsorption isotherms at three different temperatures for C_3H_8 and C_3H_6 are 34.5 and 31.2 kJ/mol (Figure 4d), respectively, confirming that the gas–framework interaction for the former is stronger than that of the latter.

IAST Selectivities and Dynamic Breakthrough Experiments. The selective adsorption of C_3H_8 over C_3H_6 by HIAM-402 was further evaluated by ideal adsorbed solution theory (IAST) for two different compositions ($\text{C}_3\text{H}_8/\text{C}_3\text{H}_6 = 1/1$ and $1/15$) (Figure 4e). The $\text{C}_3\text{H}_8/\text{C}_3\text{H}_6$ selectivity decreases as pressure increases, from 1.91 at 0.01 bar to 1.43 at 1 bar. Compared to other reported C_3H_8 -selective adsorbents, HIAM-402 demonstrated a balanced adsorption capacity and selectivity (Figure S13).^{33–36} It is noted that these selectivities are notably lower than $\text{C}_2\text{H}_6/\text{C}_2\text{H}_4$ selectivities for best-performing C_2H_6 -selective MOFs, suggesting the discrimination of physically very similar C_3H_8 and C_3H_6 molecules is much more challenging. The balanced adsorption capacity (133.3 cm^3/g for C_3H_8 at 298 K and 1 bar) and selectivity (1.43 at 298 K and 1 bar) make HIAM-402 a promising candidate for the separation of the two gases and producing highly pure C_3H_6 .

To experimentally verify the separation capability of HIAM-402, column breakthrough experiments were performed for a binary mixture of C_3H_8 and C_3H_6 ($\text{C}_3\text{H}_8/\text{C}_3\text{H}_6 = 5/95$). The breakthrough curve shows that C_3H_6 eluted out before C_3H_8 (Figure 4f). This confirms that the material can separate C_3H_8 and C_3H_6 with the former as the preferred species. The initially eluted C_3H_6 was highly pure, with a purity higher than 99.9%. Consequently, it is experimentally verified that HIAM-402 is capable of producing high-purity C_3H_6 through one-step adsorption from a binary mixture of C_3H_6 and C_3H_8 . Three successive runs of breakthrough tests demonstrated no notable loss of separation capability (Figure S14), indicating its excellent cycle performance. Breakthrough tests under humid conditions revealed no notable loss of separation capability of the compound (Figure S15), suggesting its high resistance to water. Additional breakthrough testing for a binary mixture of

$C_3H_6/C_3H_8 = 50/50$ confirmed the separation capability of HIAM-402 was retained under a relatively wide pressure range (Figure S16). To further explore if the presence of C_3H_4 would influence the separation capability of HIAM-402, breakthrough tests for a ternary mixture of $C_3H_4/C_3H_6/C_3H_8$ (2/94/4, v/v/v) were performed at 298 K. The results indicated the compound realized one-step purification of C_3H_6 from the ternary mixture (Figure S17). This is significant, as C_3H_4 is commonly present in the C_3H_6 stream but there is no report of one-step extraction of C_3H_6 from $C_3H_4/C_3H_6/C_3H_8$ mixtures prior to this work. The crystallinity and porosity of HIAM-402 after breakthrough tests were analyzed. The results indicated, after propane/propylene/propyne ternary separation experiments and after propane/propylene breakthrough tests under humid conditions, the structure and porosity of the compound were fully preserved (Figures S18–S19).

Ab Initio Calculations. To further understand the preferential adsorption of C_3H_8 over C_3H_6 by HIAM-402, we performed *ab initio* calculations to model possible adsorption sites as well as binding energies.^{37,38} C_3H_8 and C_3H_6 molecules were loaded into the already relaxed MOF structure at several positions to find the optimum binding locations. It is observed that the most favorable site for both guest molecules is in between the metal clusters (Figure 5). The incremental binding energies for C_3H_6 and C_3H_8 are calculated to be 31 and 37 kJ/mol, respectively. These values are in excellent agreement with our experimental Q_{st} values of 31.2 and 34.5 kJ/mol for C_3H_6 and C_3H_8 , respectively. The induced charge density was calculated to further visualize the guest–host (and guest–guest) interactions (Figure S20). The main interaction of the guest molecules is observed with the terminal OH and H_2O , through C–H...H interactions and CH...O hydrogen bonds. Furthermore, due to shorter H@ C_3H_8 bonds with terminal OH and H_2O , we see a stronger interaction of C_3H_8 with the framework. This explains the preferential adsorption of C_3H_8 over C_3H_6 by the framework.

CONCLUSIONS

In summary, we present in this work three new MOF structures with different topologies, built on hexanuclear Zr_6/Y_6 clusters and a tetracarboxylate linker. The different networks of the MOFs originate from the distinctly different geometries of their inorganic SBUs as well as the organic linker. This also leads to different porosity and framework stability of the three compounds. In particular, HIAM-402 with **sqc** topology features high stability and large porosity, and more importantly, it exhibits preferential adsorption of C_3H_8 over C_3H_6 . Dynamic breakthrough experiments confirmed that the adsorbent can achieve one-step purification of C_3H_6 from a binary mixture. The thermodynamically driven separation mechanism was further confirmed by *ab initio* calculations. Our study demonstrates that constructing MOFs through regulation of SBU and ligand configuration/geometry could be a general approach for achieving more functional materials for various applications.

ASSOCIATED CONTENT

Supporting Information

The Supporting Information is available free of charge at <https://pubs.acs.org/doi/10.1021/jacs.2c09487>.

Materials synthesis, methods and experimental details, crystal structure data (CCDC Numbers: HIAM-402,

2205067; HIAM-403, 2205065; HIAM-311, 2205066), and material stability characterization (PDF)

Accession Codes

CCDC 2205065–2205067 contain the supplementary crystallographic data for this paper. These data can be obtained free of charge via www.ccdc.cam.ac.uk/data_request/cif, or by emailing data_request@ccdc.cam.ac.uk, or by contacting The Cambridge Crystallographic Data Centre, 12 Union Road, Cambridge CB2 1EZ, UK; fax: +44 1223 336033.

AUTHOR INFORMATION

Corresponding Authors

Hao Wang – Hoffmann Institute of Advanced Materials, Shenzhen Polytechnic, Shenzhen, Guangdong 518055, P. R. China; orcid.org/0000-0001-7732-778X; Email: wanghao@szpt.edu.cn

Jizhao Zou – College of Materials Science and Engineering, Shenzhen University, Shenzhen 518060, P. R. China; orcid.org/0000-0002-7872-3618; Email: zoujizhao@szu.edu.cn

Jing Li – Hoffmann Institute of Advanced Materials, Shenzhen Polytechnic, Shenzhen, Guangdong 518055, P. R. China; Department of Chemistry and Chemical Biology, Rutgers University, Piscataway, New Jersey 08854, United States; orcid.org/0000-0001-7792-4322; Email: jingli@rutgers.edu

Authors

Xingyu Li – Hoffmann Institute of Advanced Materials, Shenzhen Polytechnic, Shenzhen, Guangdong 518055, P. R. China; College of Materials Science and Engineering, Shenzhen University, Shenzhen 518060, P. R. China

Jiaqi Liu – Hoffmann Institute of Advanced Materials, Shenzhen Polytechnic, Shenzhen, Guangdong 518055, P. R. China

Kang Zhou – Hoffmann Institute of Advanced Materials, Shenzhen Polytechnic, Shenzhen, Guangdong 518055, P. R. China

Saif Ullah – Department of Physics and Center for functional Materials, Wake Forest University, Winston-Salem, North Carolina 27109, United States; orcid.org/0000-0001-8836-9862

Timo Thonhauser – Department of Physics and Center for functional Materials, Wake Forest University, Winston-Salem, North Carolina 27109, United States; orcid.org/0000-0003-4771-7511

Complete contact information is available at: <https://pubs.acs.org/10.1021/jacs.2c09487>

Author Contributions

[†]X.L. and J.L. contributed equally.

Notes

The authors declare no competing financial interest.

ACKNOWLEDGMENTS

We thank the National Natural Science Foundation of China (21901166) and Shenzhen Science and Technology Program (No. RCYX20200714114539243, JCYJ20190809145615620, KCXFZ20211020163818026) for financial support. Work in the US was supported by the U.S. Department of Energy, Office of Science, Office of Basic Energy Sciences under Award No. DE-SC0019902.

REFERENCES

- (1) Furukawa, H.; Cordova, K. E.; O'Keeffe, M.; Yaghi, O. M. The Chemistry and Applications of Metal-Organic Frameworks. *Science* **2013**, *341*, 1230444.
- (2) Cadiau, A.; Adil, K.; Bhatt, P. M.; Belmabkhout, Y.; Eddaoudi, M. A metal-organic framework-based splitter for separating propylene from propane. *Science* **2016**, *353*, 137–140.
- (3) Cui, X.; Chen, K.; Xing, H.; Yang, Q.; Krishna, R.; Bao, Z.; Wu, H.; Zhou, W.; Dong, X.; Han, Y.; Li, B.; Ren, Q.; Zaworotko, M. J.; Chen, B. Pore chemistry and size control in hybrid porous materials for acetylene capture from ethylene. *Science* **2016**, *353*, 141–144.
- (4) Li, L.; Guo, L.; Olson, D. H.; Xian, S.; Zhang, Z.; Yang, Q.; Wu, K.; Yang, Y.; Bao, Z.; Ren, Q.; Li, J. Discrimination of xylene isomers in a stacked coordination polymer. *Science* **2022**, *377*, 335–339.
- (5) Mason, J. A.; Oktawiec, J.; Taylor, M. K.; Hudson, M. R.; Rodriguez, J.; Bachman, J. E.; Gonzalez, M. I.; Cervellino, A.; Guagliardi, A.; Brown, C. M.; Llewellyn, P. L.; Masciocchi, N.; Long, J. R. Methane storage in flexible metal-organic frameworks with intrinsic thermal management. *Nature* **2015**, *527*, 357–361.
- (6) Zhang, S.; Chen, Z.; Zhou, T.; Li, G. Zn Metal-Organic Framework with High Stability and Sorption Selectivity for CO₂. *Organometallics* **2022**, *41*, 829–835.
- (7) Shen, Y.; Pan, T.; Wang, L.; Ren, Z.; Zhang, W.; Huo, F. Programmable Logic in Metal-Organic Frameworks for Catalysis. *Adv. Mater.* **2021**, *33*, 2007442.
- (8) Yang, D.; Gates, B. C. Catalysis by Metal Organic Frameworks: Perspective and Suggestions for Future Research. *ACS Catal.* **2019**, *9*, 1779–1798.
- (9) Huang, L.-L.; Yu, L.; Li, B.; Li, B.-b.; Wang, H.; Li, J. Adsorption and Release of 1-Methylcyclopropene by Metal-Organic Frameworks for Fruit Preservation. *ACS Materials Lett.* **2022**, *4*, 1053–1057.
- (10) Wang, P.-L.; Xie, L.-H.; Joseph, E. A.; Li, J.-R.; Su, X.-O.; Zhou, H.-C. Metal-Organic Frameworks for Food Safety. *Chem. Rev.* **2019**, *119*, 10638–10690.
- (11) Li, B.; Dong, X.; Wang, H.; Ma, D.; Tan, K.; Jensen, S.; Deibert, B. J.; Butler, J.; Cure, J.; Shi, Z.; Thonhauser, T.; Chabal, Y. J.; Han, Y.; Li, J. Capture of organic iodides from nuclear waste by metal-organic framework-based molecular traps. *Nat. Commun.* **2017**, *8*, 485.
- (12) Liu, X.; Zhu, C.; Yin, J.; Li, J.; Zhang, Z.; Li, J.; Shui, F.; You, Z.; Shi, Z.; Li, B.; Bu, X.-H.; Nafady, A.; Ma, S. Installation of synergistic binding sites onto porous organic polymers for efficient removal of perfluorooctanoic acid. *Nat. Commun.* **2022**, *13*, 2132.
- (13) Zhang, Y.; Kang, X.; Guo, P.; Tan, H.; Zhang, S.-H. Studies on the removal of phosphate in water through adsorption using a novel Zn-MOF and its derived materials. *Arab. J. Chem.* **2022**, *15*, 103955.
- (14) Wang, S.-T.; Zheng, X.; Zhang, S.-H.; Li, G.; Xiao, Y. A study of GUPT-2, a water-stable zinc-based metal-organic framework as a highly selective and sensitive fluorescent sensor in the detection of Al³⁺ and Fe³⁺ ions. *CrystEngComm* **2021**, *23*, 4059–4068.
- (15) Lin, J.-B.; Nguyen, T. T. T.; Vaidhyanathan, R.; Burner, J.; Taylor, J. M.; Durekova, H.; Akhtar, F.; Mah, R. K.; Ghaffari-Nik, O.; Marx, S.; Fylstra, N.; Iremonger, S. S.; Dawson, K. W.; Sarkar, P.; Hovington, P.; Rajendran, A.; Woo, T. K.; Shimizu, G. K. H. A scalable metal-organic framework as a durable physisorbent for carbon dioxide capture. *Science* **2021**, *374*, 1464–1469.
- (16) Guillerm, V.; Maspoch, D. Geometry Mismatch and Reticular Chemistry: Strategies To Assemble Metal-Organic Frameworks with Non-default Topologies. *J. Am. Chem. Soc.* **2019**, *141*, 16517–16538.
- (17) Carrington, E. J.; McAnally, C. A.; Fletcher, A. J.; Thompson, S. P.; Warren, M.; Brammer, L. Solvent-switchable continuous-breathing behaviour in a diamondoid metal-organic framework and its influence on CO₂ versus CH₄ selectivity. *Nat. Commun.* **2017**, *9*, 882–889.
- (18) Xia, H.-L.; Zhou, K.; Yu, L.; Wang, H.; Liu, X.-Y.; Proserpio, D. M.; Li, J. Customized Synthesis: Solvent- and Acid-Assisted Topology Evolution in Zirconium-Tetracarboxylate Frameworks. *Inorg. Chem.* **2022**, *61*, 7980–7988.
- (19) Deng, H.; Grunder, S.; Cordova, K. E.; Valente, C.; Furukawa, H.; Hmadeh, M.; Gándara, F.; Whalley, A. C.; Liu, Z.; Asahina, S.; Kazumori, H.; O'Keeffe, M.; Terasaki, O.; Stoddart, J. F.; Yaghi, O. M. Large-Pore Apertures in a Series of Metal-Organic Frameworks. *Science* **2012**, *336*, 1018–1023.
- (20) Eddaoudi, M.; Kim, J.; Rosi, N.; Vodak, D.; Wachter, J.; O'Keeffe, M.; Yaghi, O. M. Systematic Design of Pore Size and Functionality in Isoreticular MOFs and Their Application in Methane Storage. *Science* **2002**, *295*, 469–472.
- (21) Guillerm, V.; Weseliński, L. J.; Belmabkhout, Y.; Cairns, A. J.; D'Elia, V.; Wojtas, L.; Adil, K.; Eddaoudi, M. Discovery and introduction of a (3,18)-connected net as an ideal blueprint for the design of metal-organic frameworks. *Nat. Chem.* **2014**, *6*, 673–680.
- (22) Chen, Y.; Zhang, X.; Mian, M. R.; Son, F. A.; Zhang, K.; Cao, R.; Chen, Z.; Lee, S.-J.; Idrees, K. B.; Goetjen, T. A.; Lyu, J.; Li, P.; Xia, Q.; Li, Z.; Hupp, J. T.; Islamoglu, T.; Napolitano, A.; Peterson, G. W.; Farha, O. K. Structural Diversity of Zirconium Metal-Organic Frameworks and Effect on Adsorption of Toxic Chemicals. *J. Am. Chem. Soc.* **2020**, *142*, 21428–21438.
- (23) Pang, J.; Yuan, S.; Qin, J.; Liu, C.; Lollar, C.; Wu, M.; Yuan, D.; Zhou, H.-C.; Hong, M. Control the Structure of Zr-Tetracarboxylate Frameworks through Steric Tuning. *J. Am. Chem. Soc.* **2017**, *139*, 16939–16945.
- (24) Wang, H.; Luo, D.; Velasco, E.; Yu, L.; Li, J. Separation of alkane and alkene mixtures by metal-organic frameworks. *J. Mater. Chem. A* **2021**, *9*, 20874–20896.
- (25) Liang, B.; Zhang, X.; Xie, Y.; Lin, R.-B.; Krishna, R.; Cui, H.; Li, Z.; Shi, Y.; Wu, H.; Zhou, W.; Chen, B. An Ultramicroporous Metal-Organic Framework for High Sieving Separation of Propylene from Propane. *J. Am. Chem. Soc.* **2020**, *142*, 17795–17801.
- (26) Wang, H.; Dong, X.; Colombo, V.; Wang, Q.; Liu, Y.; Liu, W.; Wang, X.-L.; Huang, X.-Y.; Proserpio, D. M.; Sironi, A.; Han, Y.; Li, J. Tailor-Made Microporous Metal-Organic Frameworks for the Full Separation of Propane from Propylene Through Selective Size Exclusion. *Adv. Mater.* **2018**, *30*, 1805088.
- (27) Zeng, H.; Xie, M.; Wang, T.; Wei, R.-J.; Xie, X.-J.; Zhao, Y.; Lu, W.; Li, D. Orthogonal-array dynamic molecular sieving of propylene/propane mixtures. *Nature* **2021**, *595*, 542–548.
- (28) Bloch, E. D.; Queen, W. L.; Krishna, R.; Zadrozny, J. M.; Brown, C. M.; Long, J. R. Hydrocarbon Separations in a Metal-Organic Framework with Open Iron(II) Coordination Sites. *Science* **2012**, *335*, 1606.
- (29) Liao, P.-Q.; Zhang, W.-X.; Zhang, J.-P.; Chen, X.-M. Efficient purification of ethene by an ethane-trapping metal-organic framework. *Nat. Commun.* **2015**, *6*, 8697.
- (30) Zhang, P.; Zhong, Y.; Zhang, Y.; Zhu, Z.; Liu, Y.; Su, Y.; Chen, J.; Chen, S.; Zeng, Z.; Xing, H.; Deng, S.; Wang, J. Synergistic binding sites in a hybrid ultramicroporous material for one-step ethylene purification from ternary C₂ hydrocarbon mixtures. *Sci. Adv.* **2022**, *8*, No. eabn9231.
- (31) Li, L.; Lin, R.-B.; Krishna, R.; Li, H.; Xiang, S.; Wu, H.; Li, J.; Zhou, W.; Chen, B. Ethane/ethylene separation in a metal-organic framework with iron-peroxo sites. *Science* **2018**, *362*, 443–446.
- (32) Lin, R.-B.; Wu, H.; Li, L.; Tang, X.-L.; Li, Z.; Gao, J.; Cui, H.; Zhou, W.; Chen, B. Boosting Ethane/Ethylene Separation within Isoreticular Ultramicroporous Metal-Organic Frameworks. *J. Am. Chem. Soc.* **2018**, *140*, 12940–12946.
- (33) Yang, L.; Cui, X.; Ding, Q.; Wang, Q.; Jin, A.; Ge, L.; Xing, H. Polycatenated Molecular Cage-Based Propane Trap for Propylene Purification with Recorded Selectivity. *ACS Appl. Mater. Interfaces* **2020**, *12*, 2525–2530.
- (34) He, C.; Wang, Y.; Chen, Y.; Wang, X.; Yang, J.; Li, L.; Li, J. Modification of the pore environment in UiO-type metal-organic framework toward boosting the separation of propane/propylene. *Chem. Eng. J.* **2021**, *403*, 126428.
- (35) Chang, M.; Ren, J.; Wei, Y.; Wang, J.-X.; Yang, Q.; Liu, D.; Chen, J.-F. A robust metal-organic framework with guest molecules induced splint-like pore confinement to construct propane-trap for propylene purification. *Sep. Purif. Technol.* **2021**, *279*, 119656.

(36) Hong, A. N.; Yang, H.; Li, T.; Wang, Y.; Wang, Y.; Jia, X.; Zhou, A.; Kusumoputro, E.; Li, J.; Bu, X.; Feng, P. Pore-Space Partition and Optimization for Propane-Selective High-Performance Propane/Propylene Separation. *ACS Appl. Mater. Interfaces* **2021**, *13*, 52160–52166.

(37) Kresse, G.; Joubert, D. From ultrasoft pseudopotentials to the projector augmented-wave method. *Phys. Rev. B* **1999**, *59*, 1758–1775.

(38) Kresse, G.; Furthmüller, J. Efficient iterative schemes for ab initio total-energy calculations using a plane-wave basis set. *Phys. Rev. B* **1996**, *54*, 11169–11186.

Recommended by ACS

Bridging and Fixing Metal–Organic Cages

Byeongchan Lee, Jinhee Park, *et al.*

OCTOBER 26, 2022
ACS MATERIALS LETTERS

READ 

Crystallographic Mapping and Tuning of Water Adsorption in Metal–Organic Frameworks Featuring Distinct Open Metal Sites

Yi Han, Nathaniel L. Rosi, *et al.*

OCTOBER 13, 2022
JOURNAL OF THE AMERICAN CHEMICAL SOCIETY

READ 

Exploring the Isorecticular Continuum between Phosphonate- and Phosphinate-Based Metal–Organic Frameworks

Soňa Ondrušová, Jan Demel, *et al.*

NOVEMBER 11, 2022
INORGANIC CHEMISTRY

READ 

Ligand-Directed Dimensionality Control over Zr-Based Metal–Organic Materials: From an Extended Framework to a Discrete Metal–Organic Cage and Macrocyclic

Chong Zhang, Wei Huang, *et al.*

SEPTEMBER 30, 2022
CRYSTAL GROWTH & DESIGN

READ 

Get More Suggestions >